Dynamic Wireless Power Transfer System for Electric Vehicles to Simplify Ground Facilities, Real-time Power Control and Efficiency Maximization

Mr. Akshay M
Dept. of Electrical and Electronics Engg.
Srinivas Institute of Technology, Mangaluru

Mrs.Veenarani A V
Dept. of Electrical and Electronics Engg
Srinivas Institute of Technology, Mangaluru

***Abstract*:- Wireless Power Transfer (WPT) is the process where electrical energy is transferred from a power source to an electrical load across an air gap using induction coils. These coils produce an electromagnetic field which sends energy from a charging base station (transmitter) to a coil on a portable device (receiver) with complete galvanic isolation. The receiver coil takes power from electromagnetic field and converts it into electrical power.**
This focuses on dynamic wireless power transfer for electric vehicles and proposes a vehicle-side control method for real-time power control and efficiency maximization. The proposed control strategy and controller design are presented based on a real-time estimation of the mutual inductance between a transmitter and a receiver. Simulations and experiments demonstrate that the proposed method can achieve the maximum efficiency and the desired power simultaneously.

1. INTRODUCTION

The transfer of energy from a source to a receiver has traditionally necessitated the use of a physical connection. Indeed, electrical grids and the power outlets span nearly the entire globe and deliver power to billions of people worldwide. Recently, there has been much interest into the area of wireless power transfer (WPT) that is the transmission of power without the need for physical connection. Research into WPT, however is nothing new as experiments in the field took place as far back as Nikola Tesla in the early 20th century.
Wireless power transfer (WPT) is one of the hottest research topics in transportation applications. In particular, a dynamic wireless power transfer (DWPT) system for electric vehicles (EVs) has gathered attention to extend the cruising distance of EVs and to reduce the size of the energy storage system. Its ground facilities are mainly composed of power source, high-frequency inverters, transmitters, and so on. As they are applied to rugged roadways over long distances, power control and efficiency maximization of wireless charging are desirable to be achieved on the vehicle side without signal communication. Although previous research has proposed simultaneous control methods of power control and efficiency maximization on the vehicle side, they have not been applied to the DWPT system. For maximizing the transmitting efficiency in the DWPT system, the mutual inductance between a transmitter and a receiver has to be estimated from the vehicle side. In this paper, an estimation method considering the vehicle-side control is proposed and applied to the simultaneous power and efficiency control. The effectiveness of the proposed method is verified by simulations and experiments.

2. WIRELESS POWER TRANSFER VIA MAGNETIC RESONANCE COUPLING

2.1 Circuit analysis:

The transmitter and the receiver coils are shown in Fig. 2.1. They are compensated by resonance capacitors for WPT via magnetic resonance coupling, which can achieve a highly efficient mid-range transmission and robustness to misalignment. In this paper, a series-series (SS) compensated circuit topology is used and its circuit diagram is shown in Fig. 2.2. The transmitter and the receiver are characterized by the inductances L_1, L_2, the series-resonance capacitances C_1, C_2, and the internal resistances R_1, R_2, respectively.$L_m$is the mutual inductance between the transmitter and the receiver.
These parameters are expressed in Table 2.1. If power source angular frequency is designed as follows:

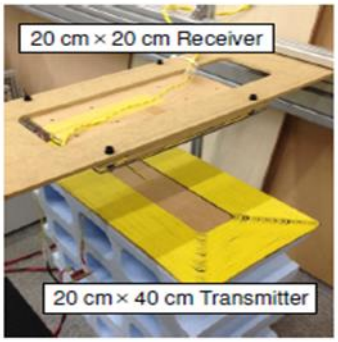

F ig 2.1: Coil

Table 2.1 : Parameters of the coil

	Transmitter	Receiver
Resistance R_1, R_2	1.95Ω	1.6Ω
Inductance L_1, L_2	417.1μH	210μH
Capacitance C_1, C_2	6030pF	12110pF
Resonant frequency f_1, f_2	100.4kHz	99.7kHz
Coil gap	100mm	
Mutual Inductance L_m	36.3μH (no misalignment)	
Coupling coefficient k	0.122 (no misalignment)	

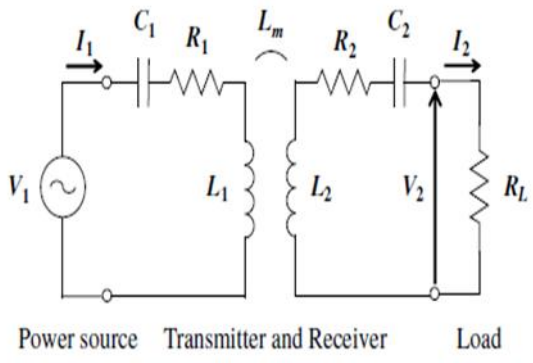

Fig. 2.3: Equivalent circuit of WPT system

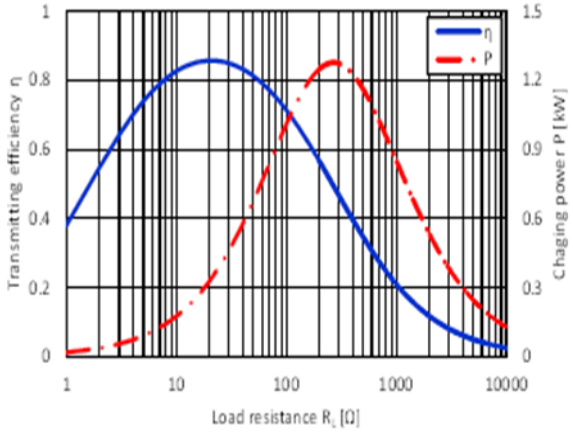

Fig. 2.4: R_L v/sη and P

$$\omega_0 = \frac{1}{\sqrt{L_1 C_1}} = \frac{1}{\sqrt{L_2 C_2}} \qquad \text{--- (2.1)}$$

The transmitting efficiency η and the transmitting power P can be obtained as follows:

$$\eta = \frac{(\omega_0 Lm)^2 RL}{R2 + RL\{R1R2 + R1RL + (\omega_0 Lm)^2\}} \qquad \text{--- (2.2)}$$

$$P = \frac{(\omega_0 Lm)^2 RL}{\{R1R2 + R1RL + (\omega_0 Lm)^2\}^2} V_1^2 \qquad \text{--- (2.3)}$$

Where V1 is the RMS value of the primary voltage and R_L is the load resistance. When VI equals to 100V, η and P are expressed in Fig 2.3. In order to maximize the transmitting efficiency η, R_L has to be given as follows:

$$R_{L\eta max} = \sqrt{R2\{\frac{(\omega_0 Lm)^2}{R1} + R2\}} \qquad \text{--- (2.4)}$$

Then, the transmitting power P is determined by$R_{\eta max}$. As a result, the desired power cannot be achieved only using R_L optimization when the transmitting efficiency η is maximized.

2.2 System configuration:

In order to achieve the maximum efficiency and the desired power simultaneously, the vehicle is equipped with two power converters, i.e. Half Active Rectifier (HAR) and the DC-DC converter. The circuit diagram of the DWPT system is shown in Fig. 2.4. The ground facility consists of voltage source V_S and an inverter, which generates a square wave voltage with resonance angular frequencyω_0. The transmitting power P is rectified by the HAR and the charging power P_L is controlled by the DC-DC converter. These control strategies and controller design methods are described below.

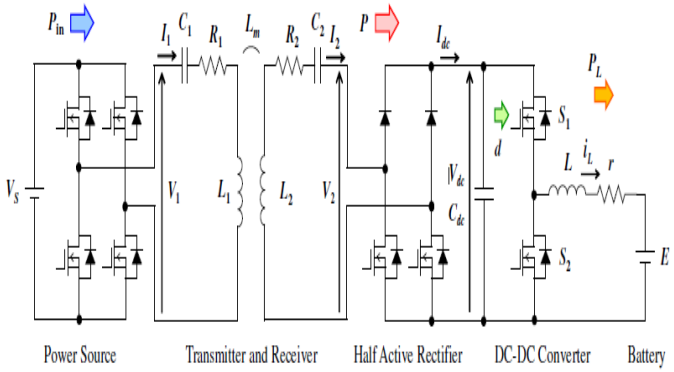

Fig 2.5: Circuit diagram of the DWPT system.

3. Efficiency Maximization by Half Active Rectifier

3.1 DC link voltage control:

The HAR regulates the DC link voltage$V_{dc}$for efficiency maximization.V_{dc}Control is achieved using two operation modes of HAR, which are shown in Fig. 3.1. When the lower arm MOSFETs are off-state, HAR is operated as the rectification mode. If the MOSFETs are turned on, HAR becomes the short mode and the receiver is shorted. Assuming the transmitting power P is larger than the load power PL,$V_{dc}$is increased during the rectification mode. On the other hand,$V_{dc}$is decreased during the short mode because P is cut-off and PL is supplied by the DC link capacitor. Therefore, the waveform ofV_{dc}can be depicted in Fig.3.2.

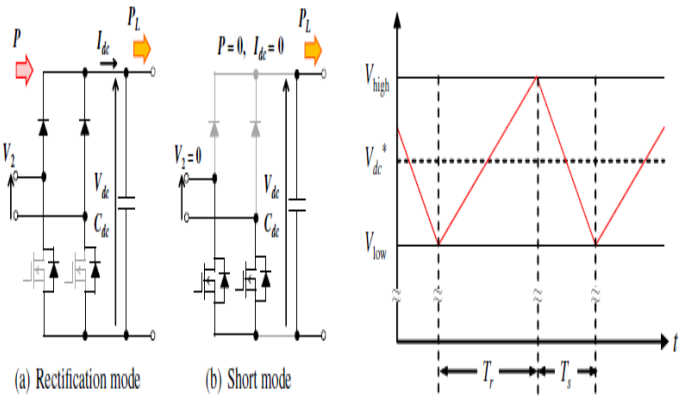

Fig 3.1: Operation modes of Half Active Rectifier.
Fig 3.2: Waveform of the DC link voltage

If the upper boundV_{high} and the lower bound$V_{low}$are defined as follows:

$V_{high} = V_{dc}^* + \Delta V$ --- (3.1)

$V_{low} = V_{dc}^* - \Delta V$ --- (3.2)

Where$V_{dc}^*$the reference value of the DC link voltage and ΔV is the hysteresis band,V_{dc} is kept within the desired range.

3.2 Efficiency Maximization:

In order to maximize the transmitting efficiency, the load resistance RL, which is expressed in Fig. 2.2 has to satisfy eq. (2.4) during the rectification mode. If$V_{dc}^*$is given as follows:

$$V_{dc\eta max} = \sqrt{\frac{R2}{R1}} \frac{\omega_0 Lm}{\sqrt{R1R2+(\omega_0 Lm)^2}+\sqrt{R1R2}} V_S \quad \text{--- (3.3)}$$

R_L is equated to$R_{L\eta max}$and the transmitting efficiency η can be maximized. On the other hand, during the short mode, the transmitting power P is drastically decreased because R_L is minimized. As a result, losses during the short mode are assumed to be negligible to losses during the rectification mode in this paper. Therefore,V_{dc}^* is determined only by$V_{dc\eta max}$.

3.3 Mutual inductance estimation:

For tracking the maximum efficiency in the DWPT system, the mutual inductance L_m has to be estimated to obtain$V_{dc\eta max}$.only using the vehicle-side information. From the circuit equations of the DWPT system, the estimation equation of L_m can be given as follows.

$$Lm = \frac{V_1+\sqrt{V_1^2-4R_1I_2(V_2+R_2I_2)}}{2I_2\omega_0} \quad \text{--- (3.4)}$$

Although eq. (3.4) has two solutions, the solution with a positive sign is used in this paper. Assuming the RMS primary voltage V_1 is constant and given to simplify ground facilities, Lm can be estimated from the vehicle side. The RMS secondary voltage $V_2$and the RMS secondary current $I_2$are calculated from the DC link voltage$V_{dc}$and the rectified DC currentI_{dc}using Fourier series expansions.

In order to reduce the estimation error due to the sensor noise, recursive least square (RLS) filter is applied. From eq. (3.4), output y[i] and regressorφ[i] are determined as follows:

$$y[i] = V_1 + \sqrt{V_1^2 - 4R_1I_2[i](V_2[i] + R_2I_2[i])} \text{--- (3.5)}$$

$$\varphi[i] = 2I_2[i]\omega_0 \quad \text{--- (3.6)}$$

RLS filter is used to estimate Lm statistically by updating Lm[i], y[i] and φ[i] with following equations.

$$Lm[i] = Lm[i-1] + \frac{\varphi[i]P[i-1]}{\lambda+\varphi[i]^2P[i-1]}\epsilon[i]$$

$$\epsilon[i] = y[i] - \varphi[i]Lm[i-1]$$

$$P[i] = \frac{1}{\lambda}\{P[i-1] - \frac{\varphi[i]^2P[i-1]^2}{\lambda+\varphi[i]^2P[i-1]}\} \quad \text{--- (3.7)}$$

Where λ is forgetting factor. The initial values are given as Lm[0] = 0 and P[0] = 1.In order to use the effective values for the estimation, the RLS filter updates Lm[i], y[i] and φ[i] only during the rectification mode of the HAR. If the HAR is operated as the short mode,I_{dc}equals to 0 andthe estimated value becomes incorrect. Therefore, the RLS filter has to be improved according to theoperation mode of the HAR.

4. POWER CONTROL BY THE DC-DC CONVERTER

4.1 Modeling of the DC-DC converter:

The DC-DC converter controls the load current $i_L$for battery charging. Assuming the DC link voltage $V_{dc}$is controlled to $V_{dc\eta max}$ by the HAR, the circuit diagram of the DC-DC converter can be expressed in Fig. 4.1 (a). E is the battery voltage, L is the inductance of the reactor coil and r is the internal resistance of the reactor coil and the battery. In this paper, the DC-DC converter model is obtained by the state space averaging method. Assuming the DC-DC converter is operated in the continuous conduction mode, its circuit diagram in each switching modes is expressed in Fig. 4.1 (b) and (c).

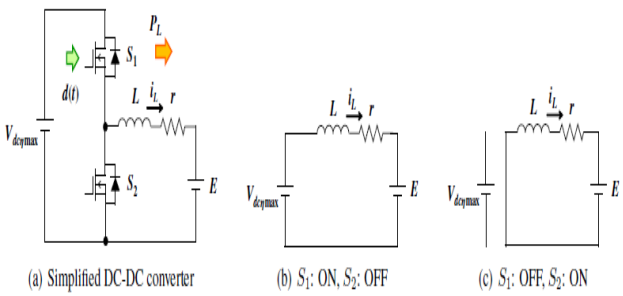

Figure 4.1: Circuit diagram of the DC-DC converter.

From the circuit equation, the state equation of Fig.4.1 (b) is given as follows:

$$\frac{d}{dt}i_L(t) = -\frac{r}{L}i_L(t) + \frac{1}{L}E + \frac{1}{L}V_{dc\eta max} \text{---(4.1)}$$

Also, the state equation of Fig.4.1 (c) is described as follows:

$$\frac{d}{dt}i_L(t) = -\frac{r}{L}i_L(t) + \frac{1}{L}E \quad \text{--- (4.2)}$$

When d(t) is defined as the duty cycle of the upper arm MOSFET S1, the state space model of the DC-DC converter is obtained as follows:

$$\frac{d}{dt}i_L(t) = -\frac{r}{L}i_L(t) + \frac{1}{L}E + \frac{V_{dc\eta max}}{L}dt \qquad \text{--- (4.3)}$$

In order to apply the linear control theory to the controller design, this model is linearized around an equilibrium point. When I_L and D are defined as the equilibrium point,$i_L(t)$ and d(t) are expressed as follows:

$i_L(t) = I_L + \Delta i_L(t)$ --- (4.4)

$d(t) = D + \Delta d(t)$ --- (4.5)

where$\Delta i_L(t)$and $\Delta d(t)$ are the microscopic fluctuations around the equilibrium point.

By substituting eq. (4.4) and eq. (4.5) in eq. (4.3), the linearized DC-DC converter model is given as follows:

$$\frac{d}{dt}i_L(t) = -\frac{r}{L}\Delta i_L(t) + \frac{V_{dc\eta max}}{L}\Delta dt \qquad \text{--- (4.6)}$$

Therefore, the transfer function from $\Delta d(s)$ to $\Delta i_L(s)$ is obtained as follows:

$$\Delta Pi(s) = \frac{\Delta i_L(s)}{\Delta d(s)} = \frac{V_{dc\eta max}}{Ls + r} \qquad \text{--- (4.7)}$$

4.2 Controller design:

Fig.4.2 shows the block diagram of the proposed control. The feed-forward controller is the same as the equilibrium point calculation, which is given by the constraint of the DC-DC converter. From$V_{dc\eta max}$,which is calculated from Lm, and the reference value of the load currenti_L^*, the equilibrium point isobtained as follows:

$I_L = i_L^*$ --- (4.8)

$$D = \frac{E + rI_L}{V_{dc\eta max}} \qquad \text{--- (4.9)}$$

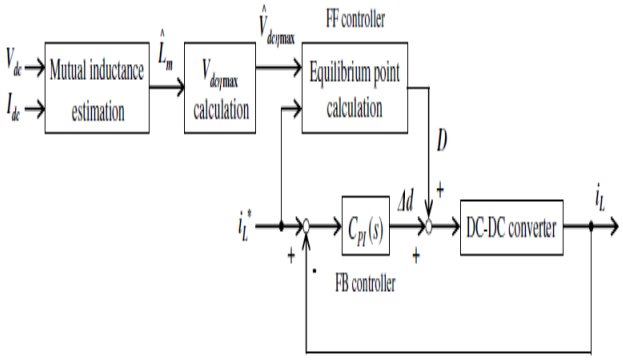

Fig. 4.2: Block diagram of the proposed control.

The feedback controller is designed by the pole placement method. As $\Delta Pi(s)$is the first-order system, we apply a PI controller$C_{PI}(s)$, which is expressed as follows:

$$C_{PI}(s) = \frac{sK_P + K_I}{s} \qquad \text{--- (4.10)}$$

If closed loop poles are given by a multiple rootω_d, the gains are obtained as follows:

$$K_P = \frac{2L\omega_d - r}{V_{dc\eta max}} \qquad \text{--- (4.11)}$$

$$K_I = \frac{L\omega_d^{\,2}}{V_{dc\eta max}} \qquad \text{--- (4.12)}$$

Here,$V_{dc\eta max}$and the gains are calculated by assuming the nominal value of $L_m$is 30Mh

5. SIMULATION AND EXPERIMENT

5.1 Experimental setup:

The experimental setup is shown in Fig. 5.1. The system configuration is the same as Table 5.1. The receiver is driven by the motor to simulate motion of the vehicle. The inverter is operated only while the receiver is above the transmitter to prevent huge power losses. Simulation and experimental conditions are expressed in Table 5.1. The forgetting factor λ of the RLS filter was set to 0.95 and the estimated mutual inductance Lm was updated only during the rectification mode of the HAR. The reference value of the DC link voltage$V_{dc\eta max}$was calculated from L_m and the reference value of the load current$i_L^*$was set to 1.0 A.

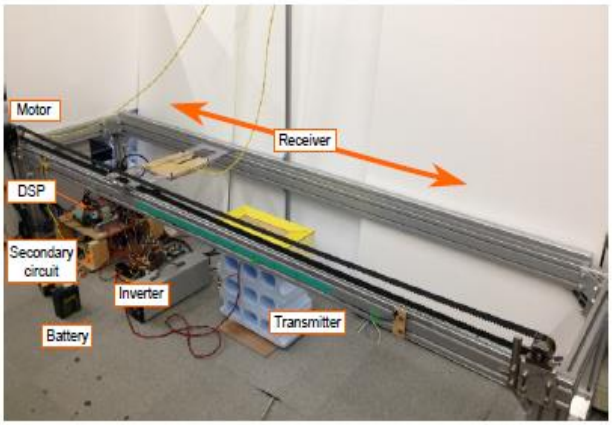

(a) Whole picture of the DWPT system.

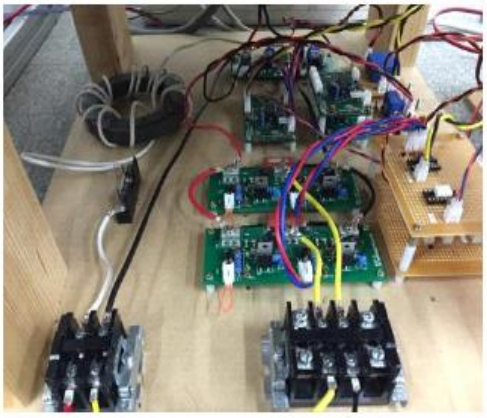

(b) Half Active Rectifier and the DC-DC converter.

Fig. 5.1: Experimental setup.

Parameter	Value	Parameter	Value
Power Source Voltage V_S	18V	Battery voltage E	6V
Operating Frequency f_0	100kHz	Reactor resistance r	0.3Ω
Hysteresis band ΔV	0.5V	Reactor Inductance L	1000μH
Carrier frequency f_c	20kHz	DC Link capacitance C_{dc}	200pF

Table 5.1: Simulation and experimental conditions.

5.2 Simulation:

In the simulations, the change in Lm was simulated by a sine wave. Its minimum and maximum values were set to 20μH and 40μH.

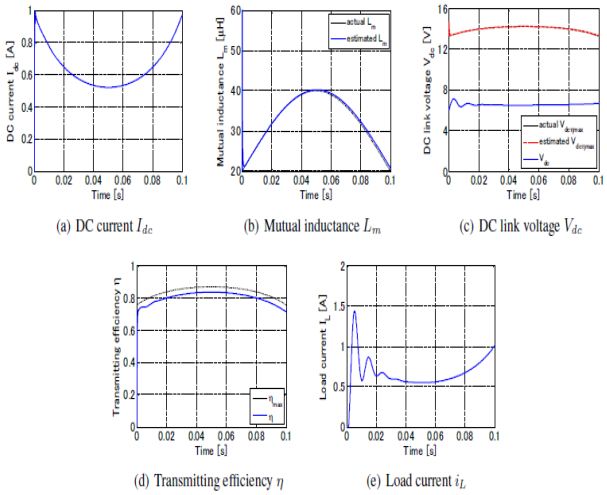

(a) DC current I_{dc} (b) Mutual inductance L_m (c) DC link voltage V_{dc}

(d) Transmitting efficiency η (e) Load current i_L

Fig. 5.2: Simulation results without the proposed control

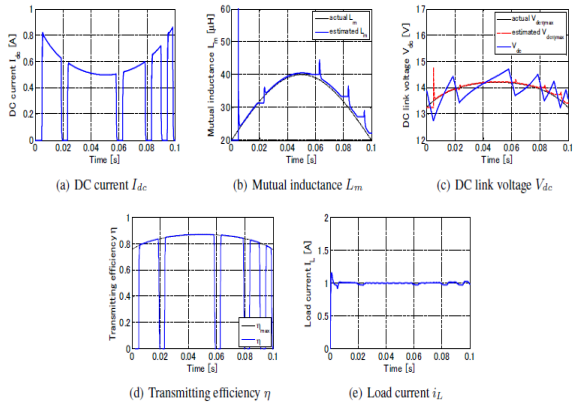

(a) DC current I_{dc} (b) Mutual inductance L_m (c) DC link voltage V_{dc}

(d) Transmitting efficiency η (e) Load current i_L

Fig. 5.3: Simulation results with the proposed control.

Fig.5.2 shows the simulation results without the proposed control. In this simulation, the HAR was operated as only the rectification mode and the duty cycle d of the DC-DC converter was equated to 0.95. From Fig.5.2 (b), L_m is closely matched with the actual L_m. However, the transmitting efficiency η is decreased from the maximum efficiency because the DC link voltageV_{dc}cannot be regulated to$V_{dc\eta max}$. Furthermore, the load current$i_L$cannot be controlled toi_L^*. Fig. 5.3 shows the simulation results with the proposed control. The closed loop poles of the proposed control were placed at -2000 rad/s. Although L_m was estimated only during the rectification mode of the HAR, L_m accords with the actual Lm as shown in Fig.5.3 (b). From Fig.5.3 (c) and (d),$V_{dc}$is regulated around$V_{dc\eta max}$and η is maximized during the rectification mode. In addition, Fig.5.3 (e) indicates that the load current control can be achieved.

5.3 Experiment:

In the experiments, the receiver was driven at 10 km/h and L_m was compared to the actual Lm, which was measured by an LCR meter (NF Corp., ZM2371). The DC to DC efficiencyη_{dc}includes not only the transmitting efficiency but also the converter efficiency because it was measured by the DC voltages and currents on each side. Therefore, improvement of system efficiency is verified in the experiments. Fig.5.4 shows the experimental results

without the proposed control. The HAR and the DC-DC converter were operated at the same condition as the simulation without control. From Fig.5.4 (b), L_m and the actual L_m are closely matched. Although Lm has a short-time delay,$V_{dc\eta max}$ is near by the actual$V_{dc\eta max}$ as shown Fig.5.4(c). However, the transmitting efficiency cannot be maximized because$V_{dc}$is not regulated to$V_{dc\eta max}$. Furthermore, Fig. 5.4 (e) indicates that$i_L$cannot be controlled unless the proposed control is applied. In the case of with control, the DC-DC converter started power control whenV_{dc}reached$V_{dc\eta max}$. The closed loop poles of the proposed control were placed at -1000 rad/s. Fig. 5.5 shows the experimental results with the proposed control. Although the error of L_m is larger than without control,V_{dc}can be controlled around$V_{dc\eta max}$ as shown in Fig. 5.5 (c). From Fig. 5.5 (d),η_{dc}during the rectification mode of the HAR is increased compared to without control. In addition, Fig. 5.5 (e) shows that$i_L$can be controlled to$i_L{}^*$. If the closed loop poles of the proposed control are optimized, it is possible to suppress the current ripple due to the fluctuation ofV_{dc}.

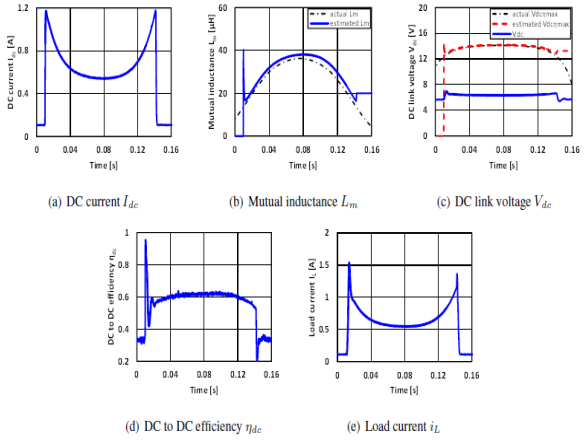

(a) DC current I_{dc} (b) Mutual inductance L_m (c) DC link voltage V_{dc}

(d) DC to DC efficiency η_{dc} (e) Load current i_L

Fig. 5.4: Experimental results without the proposed control

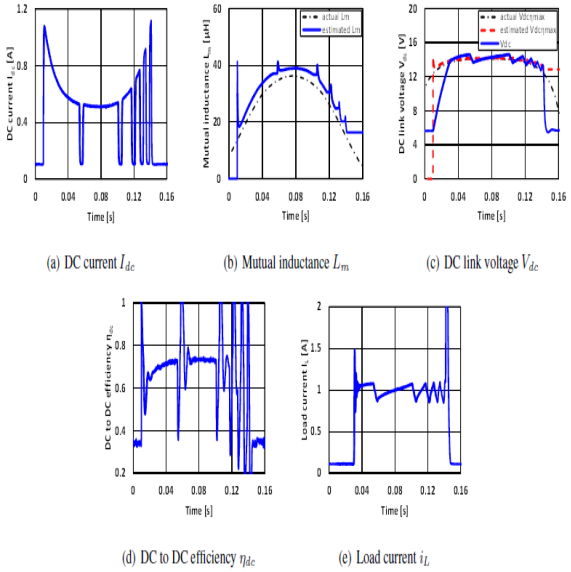

(a) DC current I_{dc} (b) Mutual inductance L_m (c) DC link voltage V_{dc}

(d) DC to DC efficiency η_{dc} (e) Load current i_L

Figure 5.5: Experimental results with the proposed control

6. CONCLUSION

This proposed a simultaneous control method of real-time power control and efficiency maximization based on improved mutual inductance estimation from the vehicle side. Its control strategy and controller design methods were presented. The effectiveness of the proposed method was verified by the simulations and the experiments. Future works are to propose an efficiency maximization method considering losses during the short mode of HAR and to design an optimal controller for the proposed control. Furthermore, the proposed method is implemented to an actual DWPT system using an EV.

REFERENCE

[1] Montr'eal, Qu'ebec, Canada, June 19-22, 2016, "Dynamic Wireless Power Transfer System for Electric Vehicles to Simplify Ground Facilities- Real time Power control and Efficiency Maximization –", Katsuhiro Hata1, Daita Kobayashi, TakehiroImura, Yoichi Hori, The University of Tokyo, 5-1-5, Kashiwa, Chiba, Japan.

[2] G. A. Covic and J. T. Boys, "Modern trends in inductive power transfer for transportation application," IEEE Journal of Emerging and Selected Topics in Power Electronics, vol. 1, no.1, pp. 28–41, Mar. 2013.

[3] S. Li and C.C. Mi, "Wireless power transfer for electric vehicle applications," IEEE Journal of Emerging and Selected Topics in Power Electronics, vol. 3, no.1, pp. 4–17, Mar. 2015.

[4] J. Shin, S. Shin, Y. Kim, S. Ahn, S. Lee, G. Jung, S. Jeon, and D. Cho, "Design and implementation of shaped magnetic-resonance-based wireless power transfer system for roadway-powered moving electric vehicles," IEEE Transactions on Industrial Electronics, vol. 61, no. 3, pp. 1179–1192, Mar. 2014.

[5] J. M. Miller, O. C. Onar, C. White, S. Campbell, C. Coomer, L. Seiber, R. Sepe, and M. Chinthavali, "Demonstrating dynamic charging of an electric vehicle: the benefit of electrochemical capacitor smoothing," IEEE Power Electronics Magazine, vol. 1, no.1, pp. 12–24, Mar. 2014.

[6] K. Lee, Z. Pantic, and S. M. Lukic, "Reflexive Field Containment in Dynamic Inductive Power Transfer Systems," IEEE Transactions on Industrial Electronics, vol. 29, no. 9, pp. 4592–4602, Sep. 2014.

[7] L. Chen, G. R. Nagendra, J. T. Boys, and G. A. Covic, "Double-coupled systems for IPT roadway applications," IEEE Journal of Emerging and Selected Topics in Power Electronics, vol. 3, no.1, pp. 37–49, Mar. 2015.

[8] G. Lovison, M. Sato, T. Imura, and Y. Hori, "Secondary-side-only simultaneous power and efficiency control for two converters in wireless power transfer system," in 41st Annual Conference of the IEEE Industrial Electronics Society (IECON), 2015, pp. 4824–4829.

[9] K. Hata, T. Imura, and Y. Hori, "Dynamic wireless power transfer system for electric vehicle to simplify ground facilities - power control and efficiency maximization on the secondary side -," in Proc. 31st Annual IEEE Applied Power Electronics Conference and Exposition, 2016, pp. 1731–1736.

[10] A. Kurs, A. Karalis, R. Moffatt, J. D. Joannopoulos, P. Fisher, and M. Soljacic,"Wirelesspowertransfer via strongly coupled magnetic resonance," Science Express on 7 June 2007, vol. 317, no. 5834, pp. 83–86, Jun. 2007.

[11] T. Imura and Y. Hori, "Maximizing air gap and efficiency of magnetic resonant coupling for wireless power transfer using equivalent circuit and Neumann formula," IEEE Transactions on Industrial Electronics, vol. 58, no. 10, pp. 4746–4752, Oct. 2011.

[12] M. Kato, T. Imura, and Y. Hori, "New characteristics analysis considering transmission distance and load variation in wireless power transfer via magnetic resonant coupling," in IEEE 34th International Telecommunications Energy Conference (INTELEC), 2012, pp. 1–5.

[13] D. Gunji, T. Imura, and H. Fujimoto, "Basic study of transmitting power control method without signal communication for wireless in-wheel motor via magnetic resonance coupling," in Proc. The IEEE/IES International Conference on Mechatronics (ICM), 2015, pp. 313–318.

[14] M. Kato, T. Imura, and Y. Hori, “Study on maximize efficiency by secondary side control using DC-DC converter in wireless power transfer via magnetic resonant coupling,” in Proc. The 27th International Electric Vehicle Symposium and Exhibition (EVS), 2013, pp. 1–5.

[15] D. Kobayashi, T. Imura, and Y. Hori, “Real-time coupling coefficient estimation and maximum efficiency control on dynamic wireless power transfer for electric vehicles,” in Proc. IEEE PELS Workshop on Emerging Technologies; Wireless Power, 2015, pp. 1–6.